A scatter and randoms weighted (SRW) iterative PET reconstruction

Ju-Chieh (Kevin) Cheng[a] and Richard Laforest
Department of Radiology, Washington University School of Medicine, St. Louis, Missouri 63110

Joseph A. O'Sullivan
Department of Electrical and Systems Engineering, Washington University, St. Louis, Missouri 63130

(Received 20 December 2010; revised 20 April 2011; accepted for publication 21 April 2011; published 31 May 2011)

Purpose: In positron emission tomography (PET) imaging, the main function of scatter and randoms corrections is to improve contrast and quantitative accuracy. Both corrections are essential and critically important. Several iterative reconstruction schemes incorporating scatter and randoms corrections have been developed over the years. In this work, the authors propose a new method to incorporate the scatter and randoms corrections into the iterative image reconstruction, which has shown promising results in regards to improving reconstruction performance and image quality as compared to the standard methods.
Methods: The authors describe a scatter and randoms weighted (SRW) iterative PET reconstruction algorithm. The SRW method is based on the estimation of the trues fraction (TF) within the *prompts*. Once the TF is estimated, it is then incorporated into the weighting component of the system matrix, and the net result is a scatter and randoms weighting in the sensitivity image similar to the attenuation correction weighting. Although using the measured *prompts* in the TF estimation was demonstrated to achieve the fastest convergence at high statistics, it is not reliable in low counts situations due to the sparse and noisy nature of the measured *prompts*. Therefore, a mean estimation of the *prompts* derived from the forward projection of the reconstructed *prompts* image was introduced into the TF estimation. A contrast phantom was scanned, and the data were reconstructed using the standard and the SRW methods.
Results: The contrast vs noise, precision vs accuracy in contrast, absolute error vs number of iterations comparisons, and standard deviation image over different realizations of the same object were evaluated at low counts situations, and it was observed that the SRW method outperforms the standard approaches such as the scatter and randoms data precorrection and the ordinary Poisson methods. The image intensity (activity) outside the object can also be minimized using the SRW method. In addition, further improvement in accuracy, precision, convergence, and noise properties can be achieved by further improving the TF and the *prompts* estimate.
Conclusions: The authors have developed a practical scatter and randoms weighting scheme in the sensitivity image for iterative PET reconstructions. Our proposed SRW method has a number of advantages over the conventional methods, and it has shown promising results with additional optimization for various applications to be further investigated. [DOI: 10.1118/1.3590379]

Key words: positron emission tomography, iterative image reconstruction, scatter and randoms corrections weighting, trues fraction within *prompts*, system matrix

I. INTRODUCTION

In positron emission tomography (PET), the data (measured *prompts*) acquired are the coincidence events or pairs of 511 keV photons generated from the positron annihilations. A pair of photons is registered as a coincidence event when the two photons are detected nearly simultaneously (within the coincidence timing and energy windows), and a corresponding line-of-response (LOR) is assigned. Scattered events occur due to the Compton scatter, which is the dominant photon interaction with a free or outer shell electron in tissue for the 511 keV photons. Although scattered photons typically have energy lower than 511 keV, they can still be registered and contaminate the measured data due to the finite energy resolution of PET scanners. As a result, one or both of the photons get scattered off of their original paths thus causing the assigned LOR nowhere close to the actual annihilation site for the registered scattered event. On the other hand, two photons from different annihilation sites can also be registered as a coincident event when one of each pair of the annihilation photons (1) gets absorbed in the object, (2) escapes the scanner's field of view, or (3) passes through the detector without getting recorded. Consequently, the coincident event is measured by "accident" due to the finite coincidence timing window, and the assigned LOR most likely does not correspond to either of the annihilation sites (i.e., randoms events). The detection of scatter and randoms events results in loss of image contrast and quantitative accuracy, and the scatter and randoms corrections are thus essential and critically important. Several iterative image reconstruction

schemes incorporating scatter and randoms corrections have been developed over the years such as the scatter and randoms data precorrection, the ordinary Poisson (OP) algorithm,[1,2] and most recently the Monte Carlo estimation of the scatter system matrix (not including the randoms).[3] In this work, we propose a scatter and randoms weighted (SRW) iterative reconstruction algorithm, which practically incorporates any existing scatter and randoms correction sinograms into the weighting component of the system matrix similar to the attenuation correction weighting.

II. A PRACTICAL SCATTER AND RANDOMS WEIGHTED SYSTEM MODEL

The core idea of the SRW method is to estimate the "trues fraction" (TF) within the *prompts*. Typically the *prompts* in PET consist of the trues (t), randoms (r), and the scattered events (s) as given by Eq. (1) which can be rearranged to form Eq. (2):

$$prompts = t + r + s \tag{1}$$

$$prompts.(1 - \mathrm{RF}) \cdot (1 - \mathrm{SF}) = prompts \cdot \mathrm{TF} = t$$
$$0 \le \mathrm{RF} \le 1, 0 \le \mathrm{SF} \le 1, \text{ and } 0 \le \mathrm{TF} \le 1, \tag{2}$$

where RF is the randoms fraction and SF is the scatter fraction as given by Eq. (3):

$$\mathrm{RF} = \frac{r}{prompts}, \quad \mathrm{SF} = \frac{s}{prompts \cdot (1 - \mathrm{RF})} \tag{3}$$

The $(1 - \mathrm{RF})$ term is thus the nonrandoms fraction, $(1 - \mathrm{SF})$ is the nonscatter fraction, and the product of the nonrandoms and nonscatter fractions is the *TF* within the *prompts*. The RF and SF are typically defined for the whole PET scan as the global estimate of the background contamination; however, here the RF, SF, and TF are defined for each LOR in the SRW method as will be discussed shortly.

The system matrix (P_{ij}) in iterative reconstruction typically consists of three parts: a weighting component (W), which accounts for normalization (n_i) and attenuation (a_i) corrections, a geometrical component (G), which correlates the LORs or bins of the sinograms and the image voxels, and a blurring component (B) for the image space resolution modeling as given by Eq. (4):

$$P_{ij} = WGB, \quad \text{where } W = \frac{1}{n_i} \cdot \frac{1}{a_i} \tag{4}$$

The SRW method is applicable to all statistical reconstruction methods like EM, OSEM, and regularized reconstruction. Here, we performed our evaluations on the most widely used reconstruction method (OSEM). The 3D ordered subsets expectation maximization[4] (3D-OSEM) using the OP method is given by Eq. (5):

$$\lambda_j^{m,l+1} = \frac{\lambda_j^{m,l}}{\sum_{i \in s_l} P_{ij}} \sum_{i \in s_l} P_{ij} \frac{y_i}{\sum_{j=1}^{J} P_{ij} \lambda_j^{m,l} + r_i + s_i}, \tag{5}$$

where y_i is the measured data along the ith LOR within the lth subset (s_l), and $\lambda_j^{m,l}$ is the image intensity estimate in voxel j ($j = 1,\ldots, J$) at the mth iteration and lth subset. Here, the scatter and randoms correction sinograms are incorporated into the reconstruction task in the forward model.

For the SRW method once the TF is estimated for each LOR, it can then be incorporated into the weighting component of the system matrix similar to the attenuation correction factors. When incorporated into 3D-OSEM, the SRW-OSEM algorithm is given by Eq. (6):

$$\lambda_j^{m,l+1} = \frac{\lambda_j^{m,l}}{\sum_{i \in s_l} P'_{ij}} \sum_{i \in s_l} P'_{ij} \frac{y_i}{\sum_{j=1}^{J} P'_{ij} \lambda_j^{m,l}}$$
$$\text{where } P'_{ij} = W'GB \text{ and } W' = \frac{1}{n_i} \cdot \frac{1}{a_i} \cdot \frac{1}{TF_i} \tag{6}$$

The net result is a scatter and randoms weighting in the sensitivity image as the weighting component (the diagonal matrix) cancels out between the forward- and back-projection step. Consequently, the definition of the sensitivity image in the SRW-OSEM becomes the probability of a "true" voxel to be detected everywhere.

It has been observed that the image estimate is less noisy and updates more quickly (i.e., faster convergence) without the inclusion of scatter and randoms corrections in Eq. (5),[2] which is equivalent to Eq. (6) with $\mathrm{TF} = 1$ for all LORs. The 3D-OSEM without scatter and randoms corrections will be referred to as the *prompts* reconstruction from here on. Ideally, if the TF can be properly estimated with negligible noise as compared to the measured data, the convergence and noise properties of the SRW method are expected to be similar to the *prompts* reconstruction while achieving better quantitative accuracy. The SRW method also maintains the Poisson nature of the data (i.e., no data precorrections applied). Moreover, since there is no need to process through the scatter and randoms sinograms for every iteration of the reconstruction in the SRW method as compared to the OP method, the storage requirement for the reconstruction task can be reduced (note that the amount of reduction depends on the number of LORs or the size of the sinogram files for the PET scanner; e.g., scanners such as the high resolution research tomography,[5] which has a large number of LORs would benefit more from this). The computation of the update factors is also more efficient thus accelerating the reconstruction task. In addition, the proposed method practically and effectively incorporates any existing scatter and randoms correction sinograms into the sensitivity image without computationally intensive simulations such as the estimation of the full scatter system matrix (for each voxel-LOR combination) as described by Rehfeld and Alber.[3]

The TF estimate can also be used as a quality control for the scatter and randoms corrections as severe bias in both correction estimates can be easily identified in the TF sinograms. Furthermore, the SRW method can minimize the image intensity (activity) outside the object by conditioning the TF using the anatomical information (attenuation sinograms) as guidance. Ideally, the TF outside the object should be zero; however, performing summation of one over zero (i.e., singularity) or one over a very small number close to zero in the sensitivity estimation has been found to be

problematic for the LORs close to the boundary of the object and prone to introduce artifact in the image. The TF outside and close to the boundary of the object was thus determined empirically, as will be discussed in Sec. V, in order to minimize the activity outside the object due to scatter and randoms while avoiding the singularity issue.

The estimation of TF requires the scatter and randoms sinograms as well as the *prompts* sinograms. A major concern arises when estimating the TF using the measured *prompts* (i.e., the direct data-driven approach) at low counts situations since the measured *prompts* sinograms are sparse and noisy, and, therefore, the estimated TF is likely to be inaccurate. To improve the TF estimation, we used the mean estimated *prompts* derived from forward projection of the reconstructed *prompts* image followed by rescaling to minimize the difference in overall magnitude as compared to the measured *prompts*. The *prompts* reconstruction was performed using Eq. (6) and setting TF = 1 for all LORs. Examples of TF estimates and the corresponding profiles are shown in Fig. 1.

One can observe that the average TF for the uniform area is about 0.8 from the profile with 3.4×10^9 (i.e., ~300 counts per bin on average within the object) counts using the measured *prompts*; however, the TF estimated from ~100 times less statistics—i.e., 33×10^6 counts using the measured *prompts* show a noisy and underestimated profile. On the other hand, the TF obtained from 33×10^6 counts using the mean estimated *prompts* is in close agreement with that estimated from 3.4×10^9 counts using the measured *prompts*. Note that the randoms and scatter estimates used are the same for Figs. 1(b) and 1(c). It can be observed that the noise and inaccuracy in the TF are mostly contributed from the measured *prompts* as shown in Fig. 1(b).

It was also observed that the TF, SF, and RF obtained from the mean estimated *prompts* are almost always within the zero to one range without using a constraint for all the LORs within the object. Although there is inconsistency between the forward- and back-projection, the TF obtained using the mean estimated *prompts* was found to be more robust and produce more consistent results when included in the SRW method for low count situations. A few denoising techniques were also applied to improve the mean estimated *prompts* (analogous to the segmentation step in attenuation correction), as will be described in Sec. III.

As compared to the widely used OP approach, the expected advantages and challenges of the SRW method are summarized below:

Advantages

1. Faster convergence
2. Producing less noisy images when the noise in the TF estimate is negligible as compared to the measured data.
3. Accelerating the reconstruction task and reducing the storage requirement.
4. TF sinograms can be used as a quality control for the scatter and randoms estimates.
5. Minimizing the image intensity (activity) outside the object

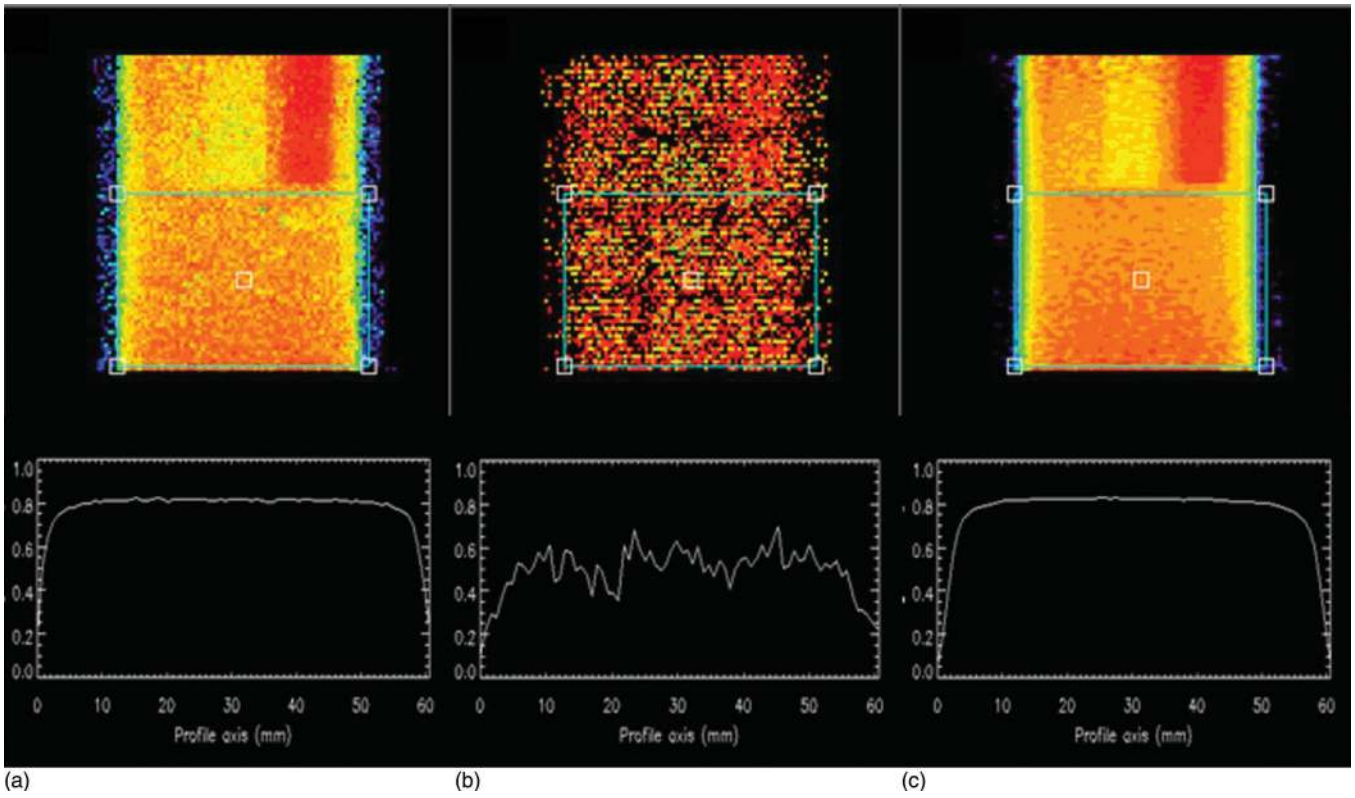

FIG. 1. The coronal "z-r" view of the TF sinograms and the corresponding profile for the contrast phantom estimated from (a) 3.4×10^9 counts with the measured *prompts*, (b) 33×10^6 counts with the measured *prompts*, and (c) 33×10^6 counts with the mean estimated *prompts*. The bright-dark pattern across the vertical axis shown in (b) is likely due to quantum fluctuations in the measured data.

Challenges

1. Singularity issue
2. Direct data-driven TF estimation is likely to be inaccurate for low counts situations; extra care is required for low-statistics reconstructions.

III. METHODS

III.A. Tomograph

Data were acquired on the microPET-Focus220. This scanner is made of four rings of block detectors composed of an array of 12×12 lutetium oxy-ortho silicate (LSO) scintillation crystals of 1.6 mm $\times$ 1.6 mm $\times$ 10 mm with optical coupling to a position sensitive photomultiplier tube via a coherent bundle of square optical fibers. The performance evaluation of this scanner was described by Tai *et al.*[6]

III.B. Data acquisition

A 6 cm in diameter and 9 cm long cylindrical phantom with a "cold" Teflon insert, a cold air insert, a "hot" water insert (each of which is 1.5 cm in diameter and 4 cm long), and a "warm" water background was scanned. The phantom was filled with a 1.36 mCi injection of a ^{18}F solution and a hot-to-background ratio of 4–1. The phantom was positioned at the center of the field of view and underwent a 6 h emission scan and an 18 min transmission scan. Data were acquired in list-mode with a total number of counts of $\sim 3.4 \times 10^9$, an average count rate of 157.4 kps, and a global RF of 11% (the count rate and RF were chosen to mimic typical conditions encountered in a small animal imaging).

III.C. Image reconstruction and comparison scheme

Data with the entire scan duration were reconstructed using eight iterations and nine subsets 3D-OSEM (1) without any scatter and randoms corrections (i.e., *prompts* recon), (2) with OP, and (3) with the proposed SRW method using the measured *prompts* (SRW_mp) in the estimation of the TF as the first step for the high statistics evaluation. The scatter and randoms corrections were computed using the single scatter simulation[7] (SSS) and the smoothed randoms estimated from singles rate.[8] Since the estimated scatter sinograms were already normalized in SSS, they need to be denormalized to match the un-normalized randoms and *prompts* before estimating the TF. The contrast for the hot insert and those for the two cold inserts was evaluated as a function of the voxel-noise in the reconstructed images and compared between the three methods mentioned above. The noise in the reconstructed image is characterized by the coefficient of variation (COV) for voxels in the background region.

The list-mode data were then sorted and divided into ten frames of 3×10^6 counts with similar count rate and RF as compared to the average count rate and the average RF. For the aforementioned low counts frames, the data were reconstructed using (1), (2), (4) the SRW method using the mean estimated *prompts* obtained using eight iterations (SRW_ep) in the TF, and additionally (5) with data precorrected for scatter and randoms (i.e., subtract the scatter and randoms from the data before reconstruction). As demonstrated in Fig. 1, the TF obtained from the mean estimate of the *prompts* was identified to be more robust as compared to the measured *prompts*; therefore, the SRW_mp method was omitted for the low counts evaluations in the result section. Furthermore, the TF obtained using the mean estimated *prompts* from the 3.4×10^9 counts frame with proper rescaling was included into the 3×10^6 counts frame reconstruction (i.e., (6) SRW_summed_ep) to demonstrate that further improvement in accuracy, precision, convergence, and noise properties can be achieved by improving the TF/*prompts* estimate. A recently developed denoising technique: HighlY constrained backPRojection[9] (HYPR), using the *prompts* image reconstructed from the 3.4×10^9 frame as the composite image, was also applied to the TF estimation process and included in the SRW method (i.e., (7) SRW_HYPR_ep) for comparison. Note that the same scatter and randoms corrections were used in all the methods mentioned above except (1). Other than the contrast vs noise comparison, the COV of the contrast values was evaluated as a function of the bias in contrast (i.e., precision vs accuracy) for all the hot and cold inserts over the ten frames. The bias in contrast is given by:

$$\mathrm{Bias}_{\mathrm{constrast}} = \left(\frac{\mathrm{Contrast}_{\mathrm{average}} - \mathrm{Contrast}_{\mathrm{reference}}}{\mathrm{Contrast}_{\mathrm{reference}}} \right) \times 100\%. \tag{7}$$

The mean absolute error in contrast was also plotted as a function of number of iterations for all methods. The mean absolute error in contrast is defined as:

$$\mathrm{MAE}_{\mathrm{constrast}} = \left(\frac{\sum_{i=1}^{N} |\mathrm{Contrast}_i - \mathrm{Contrast}_{\mathrm{reference}}|/N}{\mathrm{Contrast}_{\mathrm{reference}}} \right) \times 100\%, \tag{8}$$

where the summation goes over each realization ($i = 1,\ldots, N$) and N is the total number of realizations.

Although ideally the reference contrast is 100%, the bias and absolute error were calculated based on the reference contrasts obtained from the frame with the most statistics using SRW_mp (closest to the ideal reference as will be shown in the result section) since the contrasts obtained from the frames with lower statistics should agree with those with higher, and the consistency (both overestimation and underestimation) can be determined. The standard deviation (STD) image across the ten realizations of the same object was computed for all methods, and the image intensity outside the object was also compared between the OP and the SRW methods. In summary, the following comparisons were performed:

- Contrast vs noise
- Precision vs accuracy (i.e., COV vs bias)
- Mean absolute error vs number of iterations
- STD image
- Image intensity (activity) outside the object

In this work, we used the contrast as the main figure of merit since it is the quantity most influenced by scatter and randoms corrections.

IV. RESULTS

The contrast vs noise comparison for the scan with 3.4×10^9 counts is depicted in Figs. 2(a)–2(c). One can observe that the OP method improves the contrasts and increases the noise as compared to the *prompts* recon (i.e., no scatter and randoms corrections). Further improvement in contrasts was observed with the SRW_mp method due to the faster convergence though higher noise was also obtained (compared to the other methods at the same iteration) partly due to the faster convergence but mostly due to the noise in the measured *prompts*, which propagates through the TF estimation to the reconstructed image. Note the different convergence rate between the hot and cold regional contrasts. For the low counts evaluations as shown in Figs. 2(d)–2(i), one can observe that although the SRW_ep method performs similar in terms of accuracy with slightly worse precision as compared to OP, SRW_summed_ep outperforms all the other methods in all areas (the plots for mean absolute error vs number of iterations are not shown).

As expected, the SRW_summed_ep method shows faster convergence as well as less noise in the images as compared to the OP method. The noise in the SRW_summed_ep image was observed to be almost identical to that of the *prompts* recon when the noise in the TF estimate is negligible as compared to the noise in the data as shown in Fig. 3.

This also demonstrates that the scatter and randoms corrections do not amplify the noise in the SRW method (where each image voxel is weighted by the overall contribution of the scatter and randoms through the TF in the sensitivity) when the *prompts* estimate is not noisy, whereas the OP method increases the noise after the inclusion of scatter and randoms corrections in the forward model. The SRW_HYPR_ep method also performs quite well. As compared to OP, SRW_HYPR_ep images show similar accuracy with better precision in contrast values and less noise as well as faster convergence, and its curves fall in between those of the SRW_ep method and the SRW_summed_ep method as expected.

As depicted in Fig. 4, the comparison of STD image which represents the interframe variation shows similar results between the OP and the SRW methods with SRW_ep showing slightly higher variation and the *prompts* recon showing the highest variation. Note that the SRW methods show less variation outside the object as compared to the rest. The mean value over 24 regions-of-interest (ROI) in the warm background of the STD image is also shown. In addition, although not identical the images reconstructed with the scatter and randoms precorrections show close results as compared to those reconstructed with the OP method.

The image intensity (activity) outside the object for OP (left) and SRW (right) is shown in Fig. 5. Both images were set to have the same scale. One can observe that the image reconstructed with OP contains more counts outside the object (~5 times more on average) as compared to the SRW method.

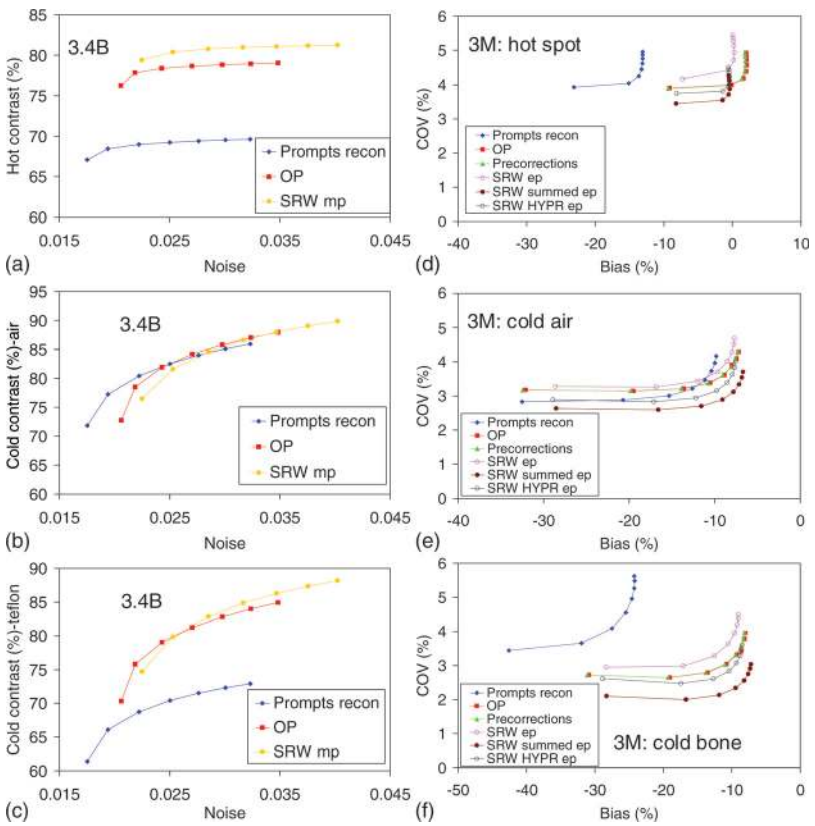

FIG. 2. Contrast vs noise comparison for (a) the hot water insert, (b) the cold air insert, and (c) the cold Teflon (bone) insert for the frame with 3.4×10^9 counts; (d), (e), and (f) depict the COV vs bias comparison for the hot water, cold air, and cold Teflon (bone) inserts, respectively, for the frames with 3×10^6 counts. Note that each point corresponds to an OSEM iteration, and the number of iterations increases from left to right.

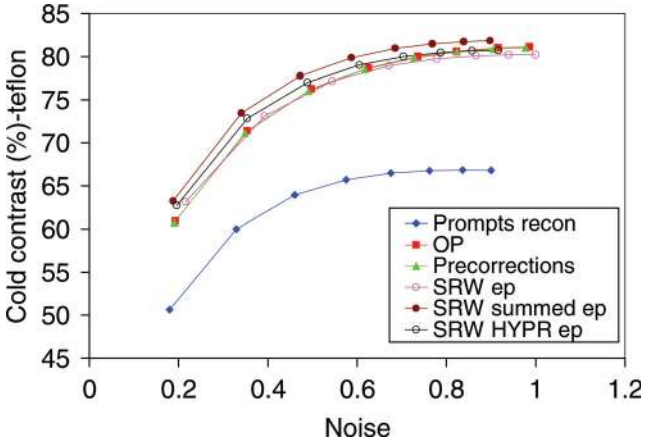

FIG. 3. Contrast (cold Teflon) vs noise comparison for the frames with 3×10^6 counts.

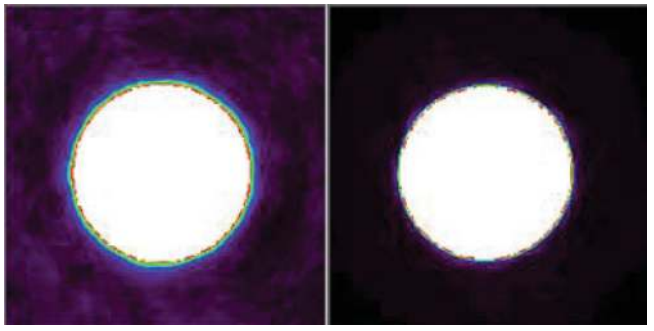

FIG. 5. The image intensity (activity) outside the object obtained with the OP method (left), and the SRW method (right); both images have the same color level scale.

V. DISCUSSION

With regard to the SRW_mp method (i.e., the direct data-driven approach), the computation of the TF is straightforward and fast as it only requires all of the existing sinograms (i.e., scatter, randoms, and measured *prompts*). In other words, the direct data-driven SRW method does not introduce any computational burden as compared to the commonly used attenuation and normalization weighted reconstruction.[10] Moreover, the reconstruction time is reduced (~15%) as compared to the OP method since there is no need to process through the scatter and randoms sinograms in the forward model for every iteration. Even though the noise obtained from the SRW_mp method is higher as compared to the other methods at the same iteration as shown in Figs. 2(a)–2(c), one can observe that with a fewer number of iterations (e.g., two iterations less) the SRW_mp method can achieve higher/similar contrasts and similar/less noise as compared to the last iteration of OP. As a result, the overall time gain becomes ~35% due to the faster reconstruction time and using a fewer number of iterations. However, the major limitation of the SRW_mp method is that it is only applicable for high statistics scans as mentioned previously. One can use the TF sinograms as the guidance to decide if the SRW_mp method is applicable as demonstrated in Fig. 1 (e.g., it is applicable when the TF sinograms are not sparse and show the structure of the object well in the z-r view). On the other hand, the SRW_ep, summed_ep, and HYPR_ep methods are suited for dynamic/low count studies. However, the reconstruction time gain is lost in the SRW_ep methods due to the additional reconstruction of the *prompts* image.

As an effort to reduce the noise in the TF estimate, we also tried incorporating the mean estimated *prompts* from earlier iterations of the *prompts* image (results not shown). Although the noise was indeed reduced in the reconstructed image, contrasts especially for the cold spots are also reduced due to the error in the TF from the reduced contrast in the early iterations of the *prompts* image (e.g., overestimated TF resulting in more counts in the cold spots). Alternatively, we used HYPR denoising technique to further improve the noise and precision properties while maintaining a good accuracy as was demonstrated by the SRW_HYPR_ep method. When we estimated the TF using the forward projection of the *prompts* image reconstructed from

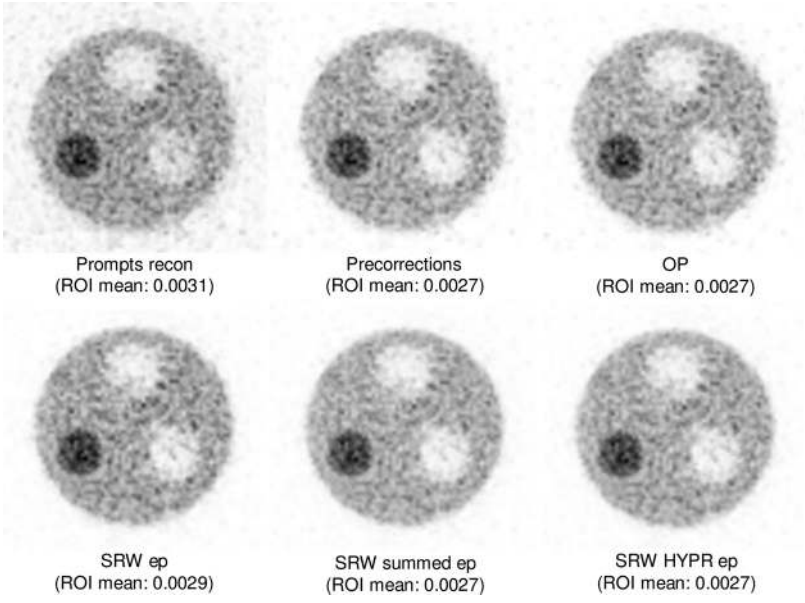

FIG. 4. The STD image comparison with the mean value from the background ROIs.

3.4×10^9 counts (i.e., SRW_summed_ep), we obtained the best results in terms of accuracy, precision, and noise. However, this approach is not generally applicable as compared to SRW_HYPR_ep since it assumes the spatial distribution of the *prompts* is constant over time. As a result, the use of SRW_summed_ep method is limited to the washout phase of tracers, where the spatial activity distribution changes minimally as well as phantom studies. In summary, even though the reconstruction time gain is lost in the SRW_ep methods, the accuracy, noise, and precision properties can be improved as compared to the other methods by improving the TF/*prompts* estimate in the SRW method. Note that the randoms and scatter estimates may also be inaccurate at low counts situations due to the limited statistics used in the estimation. Therefore, it might also be useful to apply a practical scatter and randoms approximation[11] for dynamic studies to further improve the TF estimate.

As mentioned previously, TF outside and close to the boundary of the object was determined empirically in order to minimize the activity outside the object while avoiding the singularity issue. The total image intensity (counts) outside the object for the OP method was computed and found to correspond to $\mathrm{TF} \sim 0.25$. Consequently, setting $\mathrm{TF} < 0.25$ outside the object in the SRW method improves (reduces) the background intensity as compared to OP as shown in Fig. 5. $\mathrm{TF} \sim 0.05$ outside the object has been found to be a good compromise and produce consistent results for the SRW method.

The proposed method can also be applied to the randoms precorrected data for scanners that do not have the capability to output the randoms sinograms. Instead of incorporating the TF into the weighting component of the system matrix, the nonscatter fraction (i.e., $1 - \mathrm{SF}$) should be applied for the randoms precorrected data. It is expected that the results from the scatter only weighted (SOW) method should fall in between the SRW method and the data precorrection method. Analogously, SOW can also be applied to iterative SPECT reconstruction for the scatter correction.

The proposed method has been demonstrated to work well in small animal imaging (i.e., with $\mathrm{SF} \sim 10\%$–20%). The SRW method has yet to be evaluated for human PET imaging (i.e., much higher SF). The SRW method is expected to converge even faster relative to the OP method for high SF scans since high SF slows down the convergence for the OP method though other limitations of SRW might also be discovered.

VI. CONCLUSION

We have developed a practical scatter and randoms weighting scheme in the sensitivity image for iterative PET reconstructions. Our proposed SRW method has a number of advantages over the conventional methods, and it has shown promising results with additional optimization for various applications to be further investigated. Future work for the proposed method includes further optimization for the TF/*prompts* estimate for various sizes of objects, investigation of other approaches to deal with singularity, and incorporation of additional correction terms, such as cascade gamma correction,[12,13] for nonstandard PET nuclides, and LSO background estimates for specific PET scanners, into the TF estimation. In addition, the SRW method can be extended to 4D-PET reconstruction[14] by estimating the TF from the 4D *prompts* image.

ACKNOWLEDGMENTS

The authors would like to thank Dr. Andrew J. Reader and John Floberg for their helpful discussions about the performance evaluation and the HYPR reconstruction, respectively. This work was supported by an NIH grant—the Research Resource for Cancer Applications (NIH Grant No. R24 CA86307) and by the Washington University Small Animal Imaging Resource (NIH Grant No. SAIRP R24 CA083060).

[a]Author to whom correspondence should be addressed. Electronic mail: chenj@mir.wustl.edu; Telephone: (314) 362-7215.

[1]D. G. Politte and D. L. Snyder, "Corrections for accidental coincidences and attenuation in maximum-likelihood image reconstruction for positron-emission tomography," IEEE Trans. Med. Imaging **10**, 82–89 (1991).
[2]A. Rahmim, J.-C. Cheng, S. Blinder, M.-L. Camborde, and V. Sossi, "Statistical dynamic image reconstruction in state-of-the-art high resolution PET," Phys. Med. Biol. **50**, 4887–4912 (2005).
[3]N. Rehfeld and M. Alber, "A parallelizable compression scheme for Monte Carlo scatter system matrices in PET image reconstruction," Phys. Med. Biol. **52**, 3421–3437 (2007).
[4]H. M. Hudson and R. S. Larkin, "Accelerated image reconstruction using ordered subsets of projection data," IEEE Trans. Med. Imaging **13**, 601–609 (1994).
[5]H. de Jong, F. H. van Velden, and R. W. Kloet, "Performance evaluation of the ECAT HRRT: An LSO-LYSO double layer high resolution, high sensitivity scanner," Phys. Med. Biol. **52**, 1505–1526 (2007).
[6]Y.-C. Tai, A. Ruangma, D. Rowland, S. Siegel, D. F. Newport, P. L. Chow, and R. Laforest, "Performance evaluation of the microPET focus: A third-generation microPET scanner dedicated to animal imaging," J. Nucl. Med. **46**, 455–463 (2005).
[7]C. C. Watson, "New, faster, image-based scatter correction for 3D PET," IEEE Trans. Nucl. Sci. **47**, 1587–1594 (2000).
[8]C. W. Stearns, D. L. McDaniel, S. G. Kohlmyer, P. R. Arul, B. P. Geiser, and V. Shanmugam, "Random coincidences estimation from singles event rates on the discovery ST PET/CT scanner," in *Proceedings of the Conference Record* (IEEE Nucl. Sci. Symp. Conf, Rec., Portland, OR, 2003), pp. 3067–3069.
[9]B. T. Christian, N. T. Vandehey, J. M. Floberg, and C. A. Mistretta, "Dynamic PET denoising with HYPR processing," J. Nucl. Med. **51**, 1147–1154 (2010).
[10]C. Michel, M. Sibomana, A. Boi, X. Bernard, M. Lonneux, M. Defrise, C. Comtat, P. E. Kinahan, and D. W. Townsend, "Preserving Poisson characteristics of PET data with weighted OSEM reconstruction," IEEE Nucl. Sci. Symp. Conf. Rec. **2**, 1323–1329 (1998).
[11]J.-C. K. Cheng, A. Rahmim, S. Blinder, M.-L. Camborde, K. Raywood, and V. Sossi, "A scatter-corrected list-mode reconstruction and a practical scatter/random approximation technique for dynamic PET imaging," Phys. Med. Biol. **52**, 2089–2106 (2007).
[12]R. Laforest and X. Liu, "Cascade removal and microPET imaging with 76Br,," Phys. Med. Biol. **54**, 1503–1531 (2009).
[13]J.-C. Cheng, N. Agbeko, J. O' Sullivan, and R. Laforest, "Evaluation of an iterative cascade gamma ray correction algorithm for non-standard PET nuclides at various counting statistics in high resolution small animal PET imaging,," in *Proceedings of the Conference Record* (IEEE Nucl. Sci. Symp. Conf. Rec., Orlando, FL, 2009), pp. 2842–2845.
[14]A. Rahmin, J. Tang, and H. Zaidi, "Four-dimensional (4D) image reconstruction strategies in dynamic PET: Beyond conventional independent frame reconstruction," Med. Phys. **36**, 3654–3670 (2009).